Developmental Biology 325 (2009) 374–385

Contents lists available at ScienceDirect

Developmental Biology

journal homepage: www.elsevier.com/developmentalbiology

Dependence of myoblast fusion on a cortical actin wall and nonmuscle myosin IIA

Rui Duan, Patricia J. Gallagher *

Department of Cellular and Integrative Physiology, Indiana University School of Medicine, 635 Barnhill Drive, Indianapolis, IN 46202-5120, USA

ARTICLE INFO

Article history:
Received for publication 9 May 2008
Revised 23 October 2008
Accepted 27 October 2008
Available online 5 November 2008

Keywords:
Myoblast fusion
Nonmuscle myosin II
Actin
Skeletal muscle development
Vesicle pairing

ABSTRACT

Cell–cell fusion is a fundamental cellular process that is essential for development as well as fertilization. Myoblast fusion to form multinucleated skeletal muscle myotubes is a well studied, yet incompletely understood example of cell–cell fusion that is essential for formation of contractile skeletal muscle tissue. Studies in this report identify several novel cytoskeletal events essential to an early phase of myoblast fusion among cultured murine myoblasts. During myoblast pairing and alignment, cortical actin filaments organize into a dense actin wall structure that parallels and extends the length of the plasma membrane of the bipolar, aligned cells. As fusion progresses, gaps appear within the actin wall at sites of vesicle accumulation, the vesicles pair across the aligned myoblasts, cell–cell contacts and fusion pores form. Inhibition of nonmuscle myosin IIA (NM-MHC-IIA) motor activity prevents formation of this cortical actin wall, as well as the appearance of vesicles at a membrane proximal location, and myoblast fusion. These results suggest that early formation of a subplasmalemmal actin wall during myoblast alignment is a critical event for myoblast fusion that supports bipolar membrane alignment and temporally regulates trafficking of vesicles to the nascent fusion sites during skeletal muscle myoblast differentiation.

Introduction

Cell–cell fusion is a fundamental process needed for development and formation of multicellular organisms, yet the molecular mechanisms that regulate this process are not well understood. There are numerous examples of cell–cell fusion that have been described including fertilization, bone and muscle development, and tissue regeneration. Among these examples of cell–cell fusion, the fusion of skeletal muscle myoblasts to form a multinucleated muscle fiber is an especially fascinating system that has garnered more interest recently in light of its therapeutic potential. Skeletal muscle myoblast fusion is an essential and early step required for the generation of multinucleated muscle fibers during muscle development and repair. Many studies have provided important insights regarding the mechanisms and molecular components that mediate skeletal muscle myoblast fusion. These include identification of the proteins mediating cell–cell adhesion and recognition of some primary signaling pathways that relay fusion signals from the cell membrane to the cytoskeleton (for recent reviews see Chen et al., 2007; Chen and Olson, 2004; Chen and Olson, 2005; Horsley and Pavlath, 2004). Despite these insightful studies, a complete understanding of the mechanisms governing the fusion process is lacking.

Dramatic reorganization of the cytoskeleton occurs as myoblasts maneuver through the morphological changes associated with cell–cell fusion to form multinucleated myotubes. These morphological changes include myoblast migration, elongation to a bipolar shape, membrane alignment and fusion. A number of actin-cytoskeleton associated proteins have been identified as important for skeletal muscle myoblast fusion in *Drosophila* including *Drosophila* Rac (Drac1), the DOCK180 homolog myoblast city (mbc), WASP and its interacting protein D-WIP, SCAR/WAVE, and ARP2/3 (Berger et al., 2008; Doberstein et al., 1997; Erickson et al., 1997; Kim et al., 2007; Luo et al., 1994; Massarwa et al., 2007; Richardson et al., 2007; Schafer et al., 2007). Recent studies using a T-antigen immortalized myoblast cell line have highlighted the importance of another family of actin binding proteins, the nonmuscle myosins (NM-MHC) in skeletal muscle development. This study implicated two of the three NM-MHCs, IIA and IIB in the morphological transition from triangular to elongated myoblasts (Swailes et al., 2006) and further suggested that this transition appeared to be an essential prerequisite for myoblast alignment and fusion. These studies suggest that a better understanding of the role of NM-MHCs in myoblast fusion will be essential for understanding this process.

In this report we extend these studies to identify a novel cortical actin wall, which forms in aligned, bipolar skeletal muscle myoblast cultures early during differentiation. These results demonstrate that this actin wall undergoes a dramatic reorganization prior to "vesicle paring" and fusion pore formation. Depletion of the myosin II motor,

Abbreviations: NM-MHC, non-muscle myosin heavy chain; *NM-MHC-IIA*, non-muscle myosin II, isoform A; *NM-MHC-IIB*, non-muscle myosin II, isoform B; *NM-MHC-IIC*, nonmuscle myosin II, isoform C; *RLC*, myosin II regulatory light chain; *F-actin*, filamentous actin; *G-actin*, globular actin; *EM*, electron microscopy; *TEM*, transmission electron microscopy; *siRNA*, small interfering RNA; *NT-siRNA*, non-targeting siRNA; *si-IIA*, siRNA to NM-MHC-IIA; *si-IIB*, siRNA to NM-MHC-IIB; *GM*, growth medium; *DM*, differentiation medium.

* Corresponding author. Fax: +1 317 274 3318.
E-mail address: pgallag@iupui.edu (P.J. Gallagher).

0012-1606/$ – see front matter © 2008 Elsevier Inc. All rights reserved.
doi:10.1016/j.ydbio.2008.10.035

NM-MHC-IIA strongly attenuated formation of the actin wall, as well as the subsequent appearance of vesicles at a membrane proximal location and ultimately blocks myoblast fusion. Collectively, these results suggest that NM-MHC-IIA has a critical role in driving the formation of this novel actin wall structure, which is an early prerequisite for myoblast fusion.

Results

Prefusion myoblasts develop non-uniform, cortical actin "walls"

During *in vitro* differentiation, the transition of rat L6 skeletal muscle myoblasts to prefusion myoblasts and then to multinucleated myotubes is accompanied by a dramatic reorganization of the actin filaments (Supplementary Fig. S1). During examination of optical sections (Fig. 1A) from differentiating myoblasts we identified a highly concentrated actin structure that appeared to be highly restricted to one side of the majority of the elongating myoblasts. This unusual non-uniform actin wall structure can also be appreciated in the supplementary 3-D reconstruction movie (see Movie 1 in the Supplementary material). The development of this highly organized actin wall structure was transient and it was easily detectable in myoblasts by 24 h of culture in differentiation medium (DM1) but it diminished in intensity by 48 h (DM2) and was undetectable by 96 h (DM4). The appearance of such a highly organized F-actin structure would be expected to be accompanied by a significant increase in total cellular F-actin content and a comparison of the ratio of filamentous (F) to monomeric (G) actin (Fig. 1C) revealed that between GM and DM1 there was a 93±14%

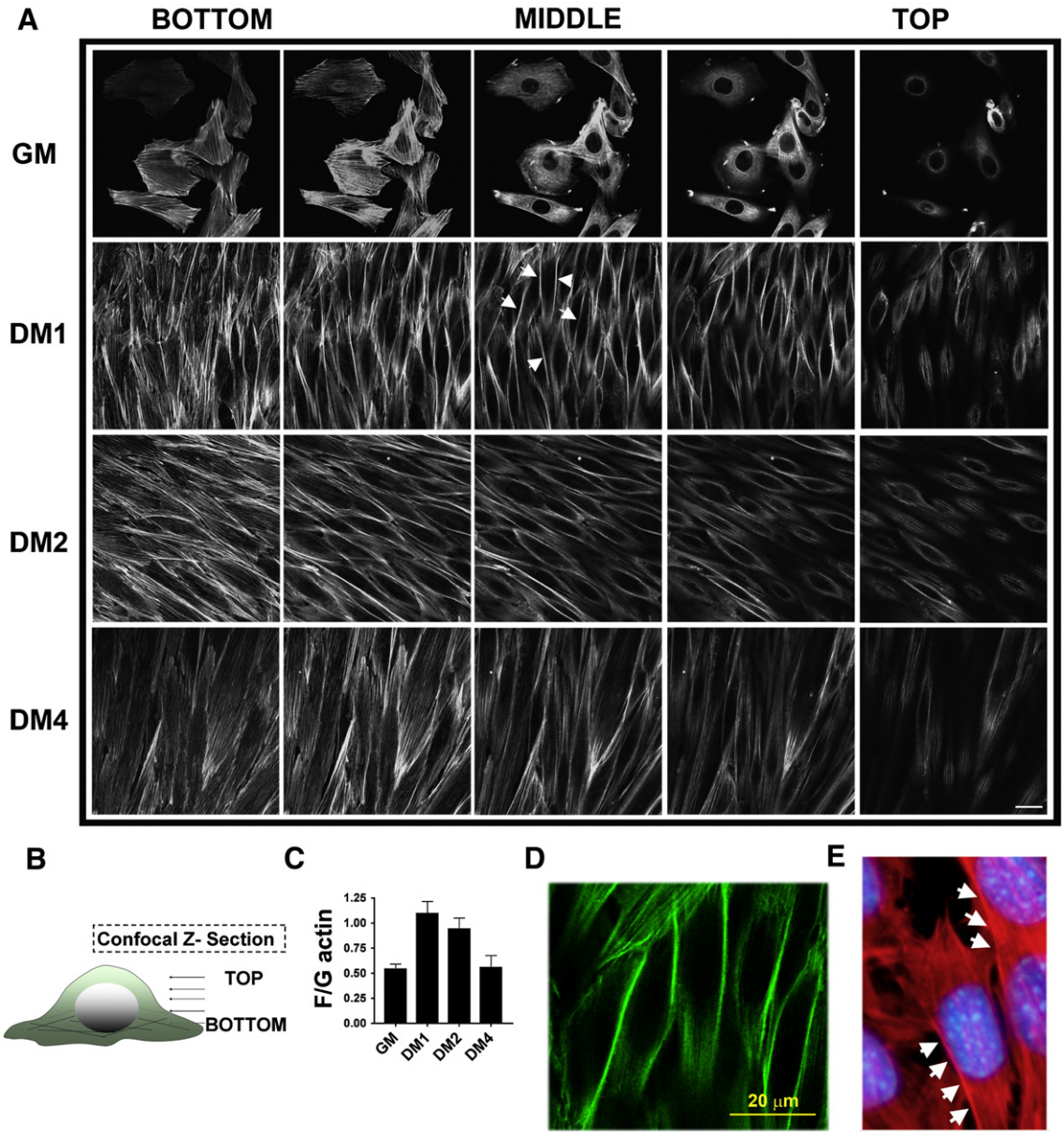

Fig. 1. Prefusion myoblasts develop non-uniform, cortical actin "walls". (A) Representative confocal projections of Z sections taken from the adherent (ventral) cell bottom, middle and proceeding upward to the media-facing top (dorsal) of L6 myoblasts. L6 myoblasts were cultured in GM or DM for the indicated times and then fixed and stained to detect F-actin using phalloidin-Alexa Fluor 488. Fluorescence images are representative of 4 independent experiments where at least 200 cells were examined per experiment. (B) Schematic illustration of location of the Z sections shown in B. (C) F-actin to G-actin (F/G) ratios during myoblast differentiation were measured following fractionation and western blotting. (D) Confocal micrographs reveal the presence of a robust, cortical F-actin wall that is present in each of the aligned L6 myoblasts. Although most of the myoblasts have this actin wall structure on one side of the bipolar cell, some myoblasts have actin walls, paralleling the entire circumference of the cell. (E) Fluorescence microscopy examination of cultures of mouse C2C12 myoblasts at DM1 revealed the presence of an actin wall (red, arrowheads) in differentiating myoblasts. The scale bar in (A) represents 50 mm and in the rest of the images represents 20 mm.

increase in F/G actin ratio. This large increase in F-actin content appears to correspond to the development of this non-uniform actin wall, as examination of z-sections from the adherent (ventral) surface as well as the top (dorsal) surface of the cells did not reveal any significant change in stress fiber organization or number. To determine if this non-uniform actin wall structure was a common feature of differentiating skeletal muscle myoblasts, 200 randomly selected pairs of aligned myoblasts in DM1 were examined in differentiating populations of L6 and C2C12 myoblasts. This study revealed that 87±3% of the L6 and 81±4% of the C2C12 myoblasts have a thick actin wall paralleling the long axis of the juxtaposed, aligned myoblasts (Figs. 1D and E). These results confirm that this non-uniform actin wall structure is a common feature of differentiating cultured murine myoblasts.

To further understand the nature of this actin structure, the subcellular cytoarchitecture of differentiating L6 skeletal muscle myoblasts was examined using transmission electron microscopy (EM). Detailed examination of the membrane proximal cytoskeletal structures in electron micrographs (Figs. 2A and B and Supplementary Fig. S2) of myoblasts in DM1 revealed that a population of cortical actin filaments becomes highly organized into thick bundles running parallel to the plasma membrane. Examination of 150 randomly selected aligned myoblast pairs in electron micrographs from several different preparations revealed that the F-actin filaments form a continuous wall-like structure that is aligned parallel to the plasma membrane and extends from one end to the other of the elongated myoblast. Measurements ($n=105$) of the thickness of the actin wall at randomly selected positions spanning the entire length of approximately 20 myoblasts in DM1, revealed that the average wall thickness was 378±109 nm. To confirm that the filaments within the actin wall are F-actin, the individual filament diameters were measured. This analysis revealed that the average diameter of each filament was 7–9 nm wide and this diameter is consistent with the identification of these filaments as actin filaments (Fowler and Aebi, 1983). Consistent with the confocal micrographs shown in Fig. 1, the cortical F-actin wall structure observed in the electron micrographs was visible only in one of a pair of adjacent aligning myoblasts, (Figs. 2A and B). The F-actin

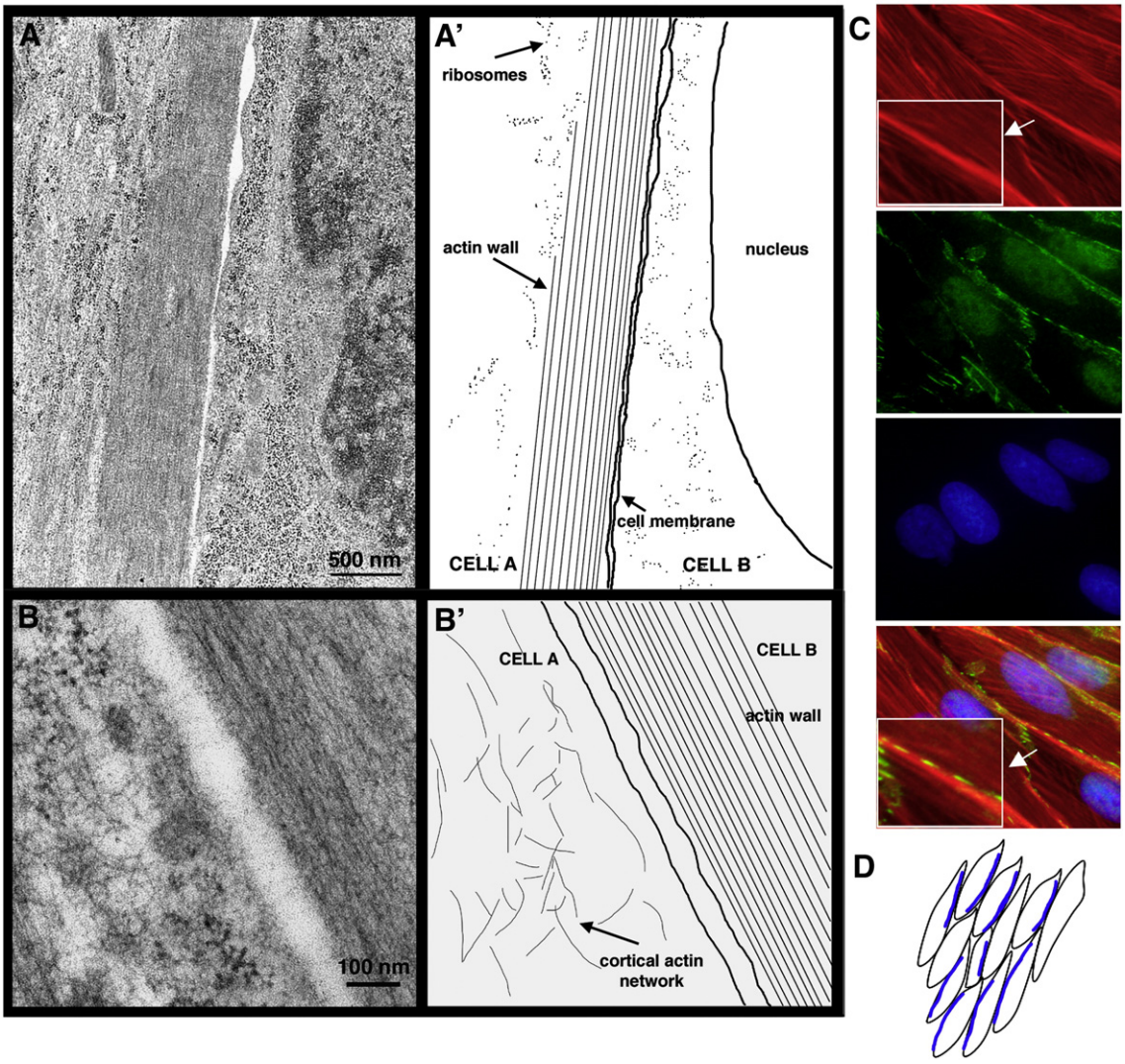

Fig. 2. Actin wall ultrastructure in differentiating skeletal muscle myoblasts. Representative transmission electron or fluorescence micrographs of L6 myoblasts cultured for 24 h in DM (DM1). (A) Transmission electron micrographs showing a highly organized bundle of actin filaments forming a continuous wall along one side of the aligned membranes of differentiating myoblasts. For additional electron micrograph images see Fig. S2 in the Supplementary material. (B) Representative transmission electron micrographs illustrating two distinct F-actin configurations that occur along the juxtaposed myoblast membranes. Cortical actin networks or meshwork are readily visible in cytoplasm of the cell on the left (cell A) and thick, parallel bundles of F-actin filaments are visible in the cell on the right (cell B). Schematic representations of these micrographs are shown in panels (A′) and (B′). Electron micrographs are representative of 3 independent preparations where at least 50 myoblast cell pairs from several different sections were examined per experiment. (C) The adherens junction marker, β-catenin (green) was used to define cell–cell contact sites, and reveals the non-uniform nature of the actin wall (red). Nuclei (blue) were detected using Hoechst 33342. (D) Schematic representation of organization of the actin wall structure in aligned myoblasts. Most of the bipolar myoblasts have a single, non-uniformly distributed actin wall that parallels one edge of plasma membrane.

filaments of the neighboring aligned myoblast were randomly oriented, resembling those found in typical cortical actin structures (Fig. 2B, cell "A").

To identify the cortical position of the actin wall structure, immunofluorescence microscopy was used to examine differentiating L6 myoblasts to detect the localization of the adherens junction marker, β-catenin as well as F-actin. Representative micrographs shown in Fig. 2C, highlight the striking asymmetry of the actin wall. In these micrographs β-catenin is used as a reference point to visualize the plasma membrane relative to the subplasmalemmal actin wall and the inset of the lowest micrograph shows a thick actin wall (red), bounded on one side by adherens junctions enriched in β-catenin (green). Collectively these data show that prior to myoblast fusion a cortical actin wall forms along the longitudinal axis of one of a pair of aligned myoblasts. The structure of this unique, non-uniform actin "wall" is distinct from typical cortical actin filament structures in that it is comprised of parallel bundles rather than randomly oriented actin filaments.

Membrane bound vesicles populate gaps within the actin wall

Results from confocal micrographs shown in Fig. 1, suggested that the actin wall appeared to disassemble or disperse during between DM2 and DM4 when the differentiating myoblast cultures enter the rapid fusion phase. To examine structural changes within the non-uniform actin wall, a three-dimensional (3D) confocal reconstruction was performed on the differentiating skeletal muscle myoblasts at DM2. Fig. 3A shows a single angle view from the reconstruction movie (see Movie 2 in the Supplementary material) and reveals the presence of several gaps within the non-uniform actin wall structure (green) in differentiating rat L6 myoblasts. To confirm this, 150 pairs of cells from 3 independent preparations were examined in electron micrographs. Fig. 3B, shows a representative micrograph where two adjacent areas within the actin wall have been enlarged. One of the enlarged regions (Fig. 3B2) shows a typical, highly organized actin wall structure and the opposing aligned myoblast, which lacks an actin wall. The second enlarged region (Fig. 3B1), which is located within 3 μm from the first

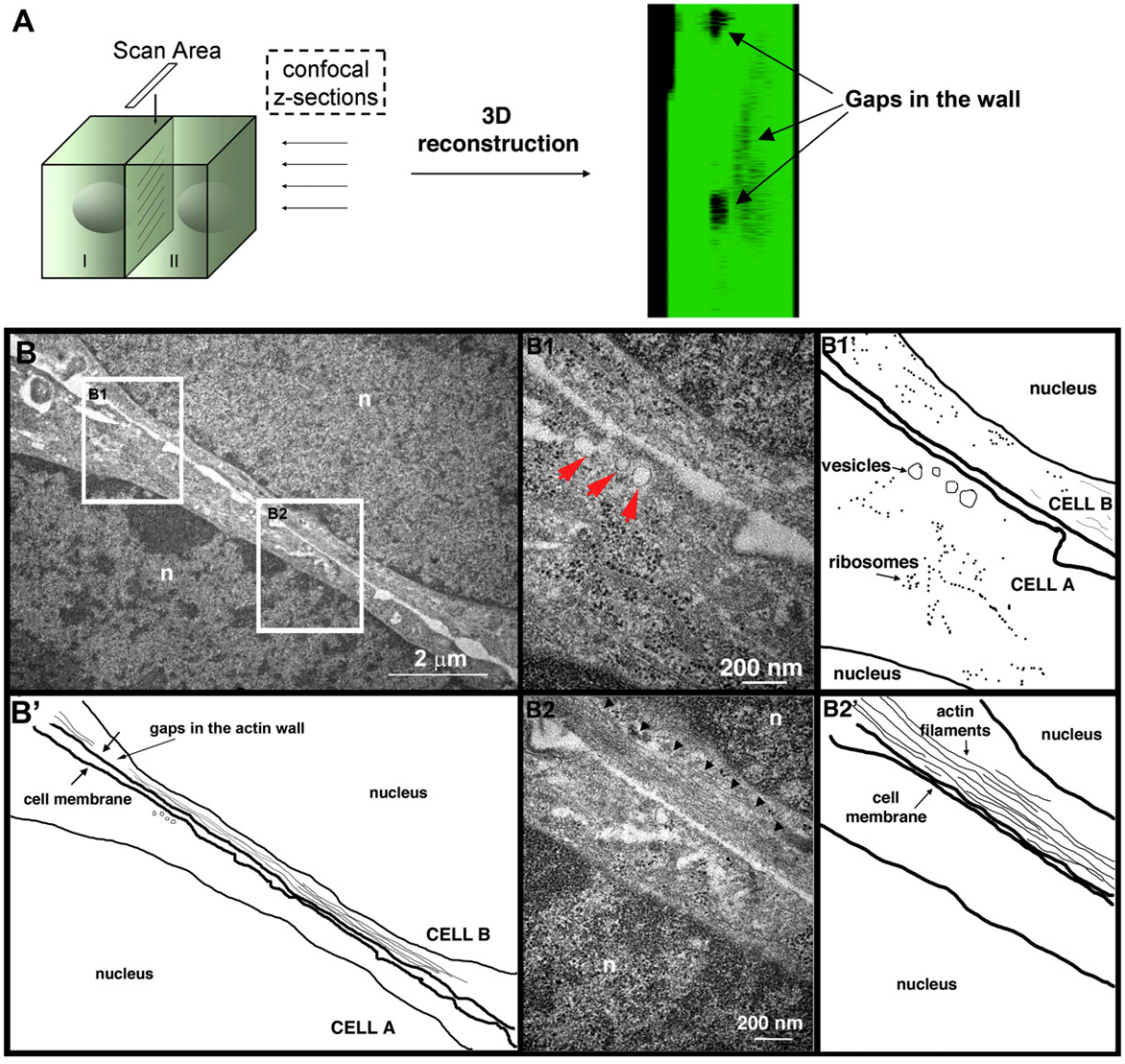

Fig. 3. Membrane bound vesicles populate gaps within the actin wall. (A) The schematic indicates the relative scan area and positioning of the confocal optical sections used for the 3D reconstruction (see Movie 2 in the Supplementary material) of an actin wall within a pair of aligned myoblasts after culture for 48 h in DM (DM2). The image (right) is a single angle view from the 3D reconstruction, which reveals the presence of several obvious gaps (black) within the actin wall (green). (B) Representative transmission electron micrographs highlighting the presence of gaps within the wall of L6 myoblasts in DM2. Cell B has an actin wall which is discontinuous along the length of the plasma membrane, while Cell A lacked any evidence of an actin wall structure. The red arrows in (B1) highlight vesicles in cell A that have aligned with the plasma membrane and are juxtaposed with a gap that present in the actin wall of cell B. The black arrowheads in (B2) highlight the actin filaments from the disintegrating wall in cell B.

enlarged region, shows a gap in the highly organized actin wall filament structure. Notably nearly all (89±4%) of the gaps observed within the wall were populated by membrane bound vesicle-like structures (Figs. 3B1 red arrows; B1′). This result suggests that the formation of gaps within the actin wall is accompanied by the migration of membrane bound vesicles to these gap areas.

Intriguingly, it was also noted that some of the vesicles within the gaps come close to contacting the plasma membrane and appear to form pairs with vesicles at the plasma membranes of the opposing aligned myoblast pair (Fig. 4, red double arrowheads). In addition, in some of the regions where clusters of vesicle pairs are evident (Fig. 4, red arrows), and there were also rare, but obvious sites where the plasma membranes of the aligned myoblasts appear to merge and have begun to form a pore-like structure (Fig. 4, blue arrow). In all of the regions where vesicles were observed to accumulate, the actin wall structure did not appear to be present. Consistent with this, in other regions of the aligned myoblasts where the actin wall is still apparent there are few or no vesicles (Figs. 3B2, B2′). In addition to the actin wall, gap formation, and appearance of vesicles in these micrographs, it was also noted that the distance between the membranes of the aligning myoblasts also was not uniform along the entire length of the aligned myoblasts, although there were numerous detectable contact sites between the aligned cells. This observation may suggest that until firm contact sites are formed or until membrane fusion is more extensive, the aligned membranes of the biopolar myoblasts may separate during preparation of the cells for EM. Together the temporal sequence of ultrastructural changes visualized in these micrographs suggests that subsequent to the formation of an actin wall, actin filaments within the wall reorganize or depolymerize to result in gaps where membrane bound vesicles accumulate. These membrane bound vesicles assemble in pairs, bridging the juxtaposed myoblast membranes and may precede the formation of fusion pores where the cytoplasm of both cells becomes contiguous.

NM-MHC-IIA is essential for myoblast fusion

A recent finding by Swailes et al. (2006) suggested that non-muscle myosin IIA (NM-MHC-IIA) is important for bipolar shape formation owing to its preferential interaction with membrane-associated actin. We therefore examined the role of this myosin II in myoblast fusion and formation of the actin wall. To determine whether inhibition of all of the myosin II motor activity in myoblasts would alter myoblast fusion either rat L6 or mouse C2C12 myoblasts (data not shown) were treated with the myosin II inhibitor, blebbistatin (Supplementary Fig. S3) or adenovirally transduced for expression of a dominant negative myosin II regulatory light chain (Supplementary Fig. S4). Results obtained using either one of these approaches showed that myosin II motor activities are essential for myoblast fusion. Western blotting (data not shown) using isoform specific antibodies to NM-MHC-IIA, IIB, or IIC was used to determine which of the three known NM-MHCs (NM-MHC-IIA, IIB or IIC) are expressed in rat L6 skeletal muscle myoblasts. These results demonstrated that only NM-MHC-IIA and NM-MHC-IIB are expressed in myoblasts and that NM-MHC-IIC is only detectable after 48 h of culture in DM, a result consistent with previous studies (Swailes et al., 2006). To determine if either NM-MHC-IIA or NM-MHC-IIB had a specific role in myoblast fusion, silencing RNAs (siRNAs) were designed and used to individually deplete either NM-MHC-IIA or NM-MHC-IIB (si-IIA, si-IIB). Supplementary Figs. 5A and B show western blotting and qRT-PCR experiments which confirm that transfection of L6 myoblasts in GM

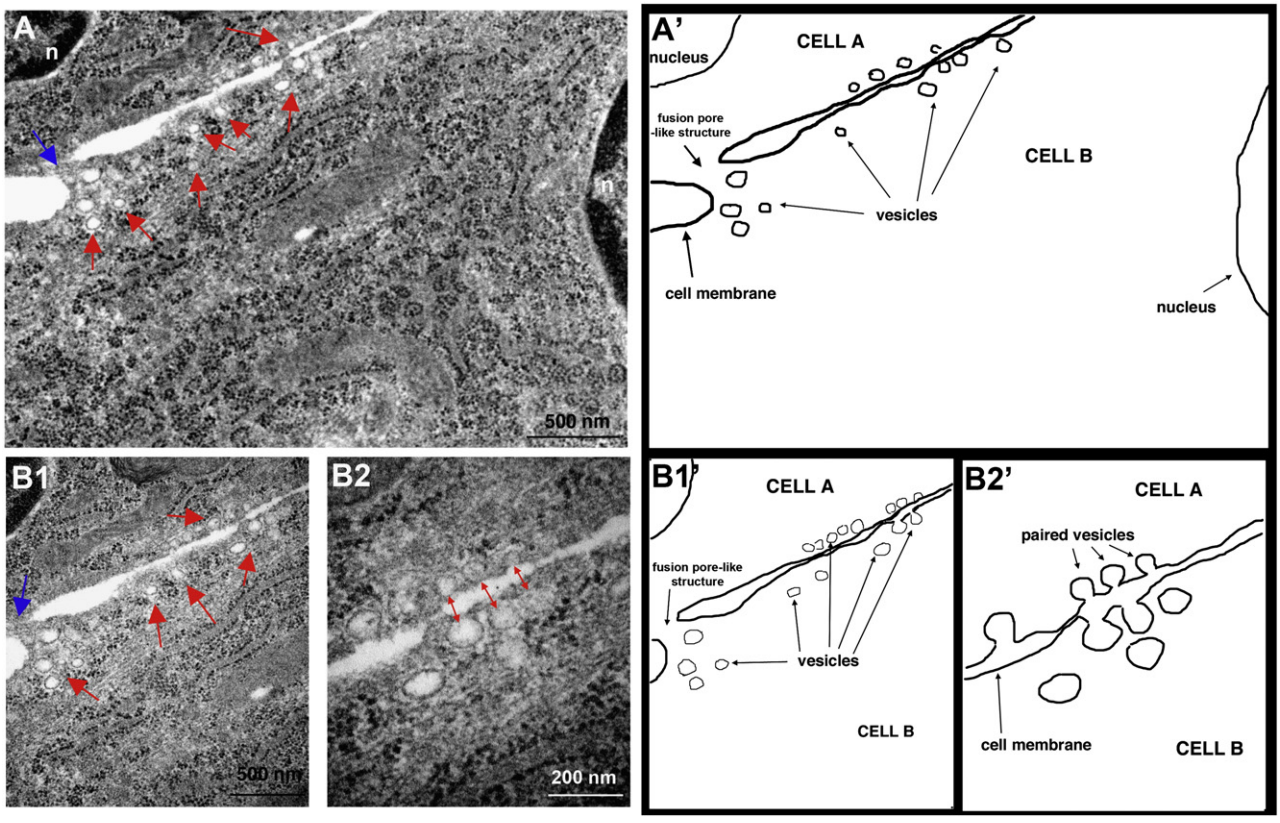

Fig. 4. Membrane bound vesicles form pairs between aligned myoblasts. Representative electron micrographs of L6 myoblasts in DM2. (A) Membrane bound vesicles (red arrows) are enriched near an apparent fusion pore (blue arrow in cell A). (B1, B2) Higher magnification (49,000× and 120,000×) micrographs of the two regions in panel (A). (B1) shows a region where membrane bound vesicles have accumulated adjacent to a fusion pore connecting the two myoblasts. (B2) highlights vesicles that have "paired" with vesicles in the opposing cell (red arrowheads). Note that in regions where nascent fusion pores are forming and vesicles are accumulating, the actin wall is undetectable. Corresponding schematic representations (A′, B1′, and B2′) highlight the nucleus, membranes, and vesicles identified in the micrographs on the left.

with an siRNA pool before the switch to DM, resulted in depletion of NM-MHC-IIA (84.5±2.1% decrease) or NM-MHC-IIB (81.3±3.4% decrease) between 2d and 4d following siRNA transfection. Using the same experimental protocol, actin filament distribution and myoblast fusion was monitored using immunofluorescence microscopy. In myoblasts depleted of NM-MHC-IIA (si-IIA) there were no obvious actin wall structures detectable in cells although prominent stress fibers were readily detectable. In contrast, myoblasts treated with si-IIB had obvious actin wall structures, which delineate the membranes of these cells (Fig. 5A). Further culture of these si-IIA treated myoblasts to DM2 or DM4 did not result in fusion to form multinucleated myotubes, while si-IIB or non-targeting siRNAs (si-NT) treated cells began fusion by DM2 and exhibited robust fusion and expression of sk-MHC by DM4 (Fig. 5B). Quantification of fusion indices (Fig. 5C) at various times following siRNA transfection confirmed that knockdown of NM-MHC-IIA resulted in a significant (86.8±2.1%) decrease in fusion after 4d of culture in DM and fewer numbers of nuclei per cell with 94.3%±2.5% of the cells having 2 or 3 nucleus (Fig. 5D). In contrast, knockdown of NM-MHC-IIB did not significantly inhibit myoblast fusion, which was indistinguishable from the fusion levels determined for myoblasts treated with transfection agent only (control) or si-NT (Fig. 5C). Interestingly, it was noted that the rare sk-MHC positive myotubes that were detected in cultures treated with si-IIA, were vastly underdeveloped having a maximum of 2 or 3 nuclei per cell (Fig. 5D). These immature myotubes were also seen in fusion-blocked myoblasts treated with blebbistatin (see Fig. S3 in the Supplementary material) or expressing a dominant negative RLC (see Fig. S4 in the Supplementary material). This low level of fusion likely results from an incomplete knockdown or inhibition of NM-MHC-IIA or alternatively could suggest that formation of precursor myoblasts with two or three nuclei is independent of NM-MHC-IIA.

Non-muscle myosin IIA is preferentially localized within the cortical actin wall

The apparent importance of NM-MHC-IIA, but not NM-MHC-IIB in formation of an actin wall in differentiating myoblasts suggested that there might be a specific association of this myosin II isoform with the wall. To determine if there was a preferential association of one of the two NM-MHC isoforms expressed in myoblasts with the cortical actin wall, L6 myoblasts were cultured in DM for 24 h before fixation and processing for immuno-electron microscopy (immuno-EM) using affinity purified, isoform specific antibodies to detect NM-MHC-IIA or NM-MHC-IIB (Gallagher et al., 2000). This analysis revealed that both NM-MHC isoforms were detectable in close proximity to the subplasmalemmal actin wall (Figs. 6A, B). However,

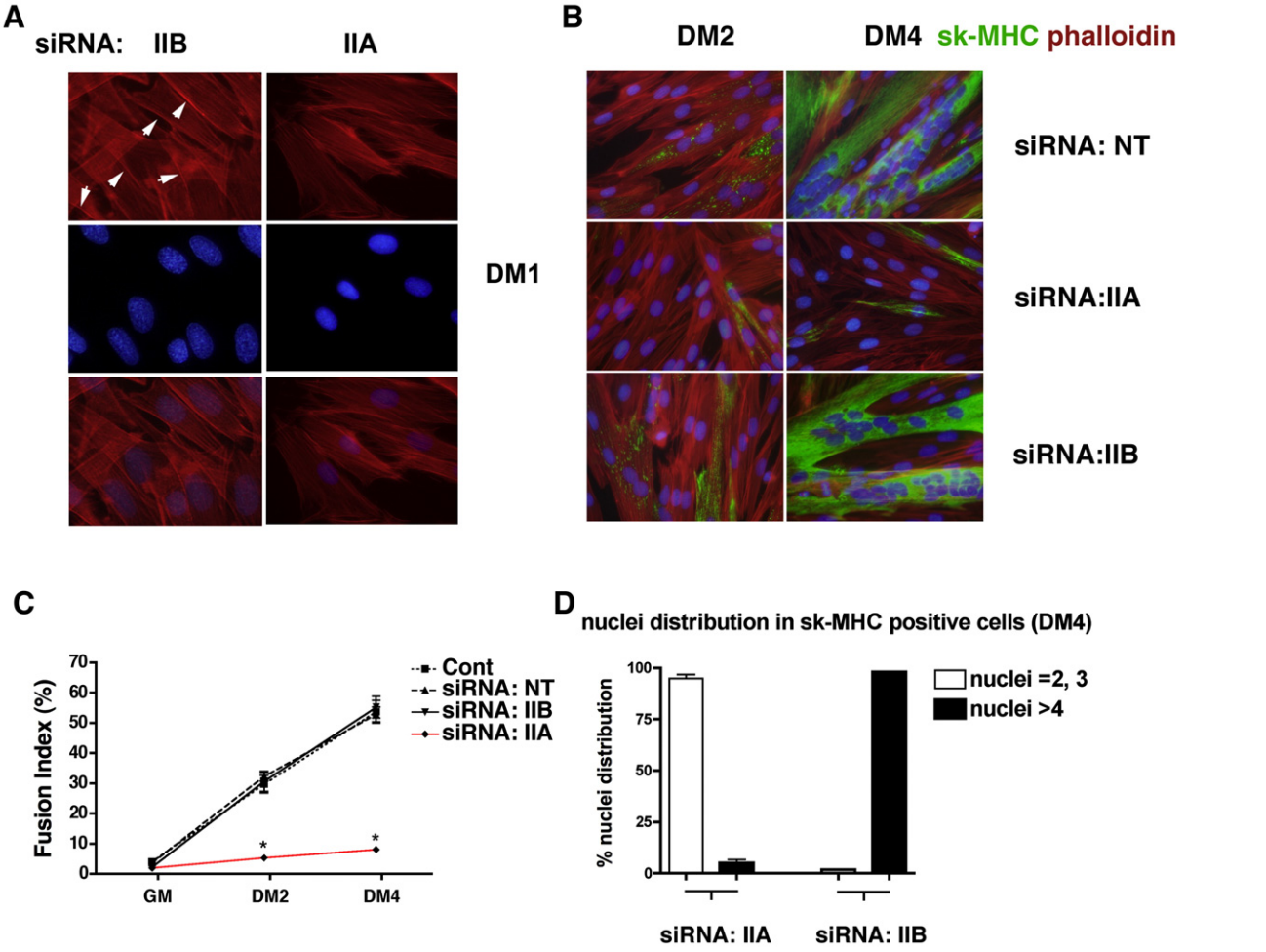

Fig. 5. NM-MHC-IIA is essential for myoblast fusion. (A) L6 myoblasts cultured in DM1 after treatment with si-IIA or si-IIB as indicated. Myoblasts deficient in NM-MHC-IIA had no obvious actin wall structures, although prominent stress fibers were readily detectable. In myoblasts deficient in NM-MHC-IIB, prominent actin wall structures, paralleling one side of the plasma membrane membranes were obvious (arrowheads). (B) L6 myoblasts cultured in DM in the presence of si-IIA, si-IIB, or si-NT for 48 (DM2) or 96 h (DM4). Myoblasts deficient in NM-MHC-IIA, but not NM-MHC-IIB or myoblasts treated with the control si-NT did not fuse to form multinucleated myotubes and do not express sk-MHC. As a measure of fusion, the number of fused myoblasts appearing in sk-MHC positive myoblasts with >4 nuclei were counted and expressed as a percent of the total number of cells counted at GM, DM2 and DM4 (C) the number of nuclei in fused myoblasts expressing sk-MHC was quantified and their distribution relative to depletion of NM-MHC-IIA or IIB is shown (D). The immunofluorescence micrographs are representative of four independent experiments. Error bars indicate mean±SD. *, $P<0.001$.

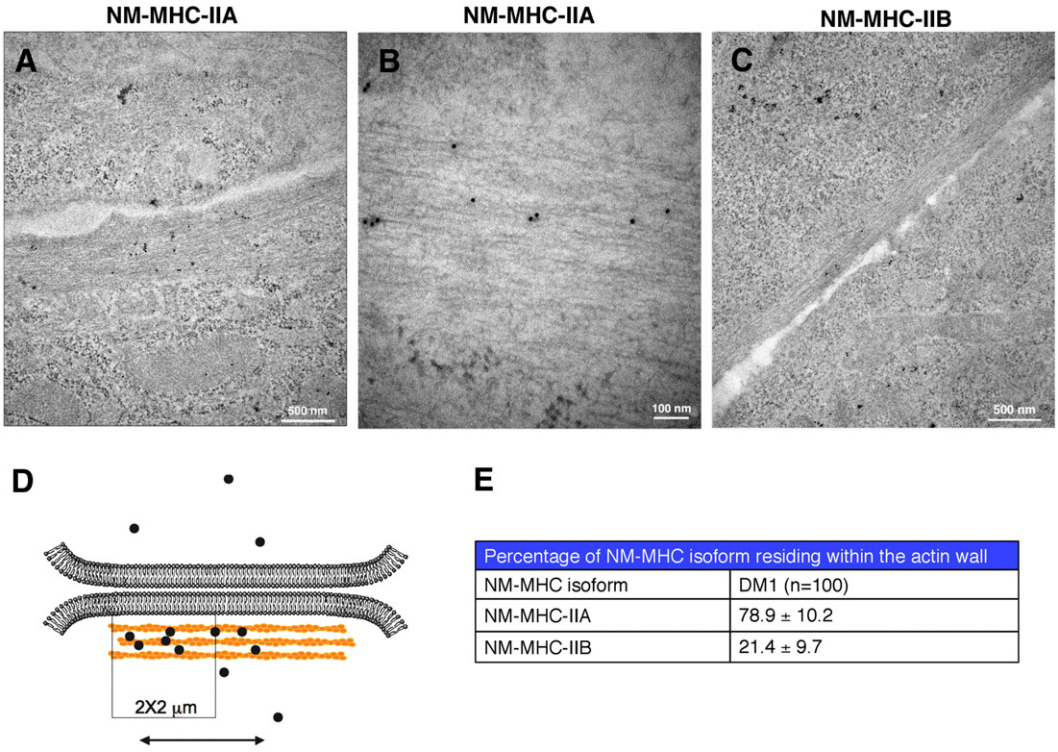

Percentage of NM-MHC isoform residing within the actin wall	
NM-MHC isoform	DM1 (n=100)
NM-MHC-IIA	78.9 ± 10.2
NM-MHC-IIB	21.4 ± 9.7

Fig. 6. Non-muscle myosin IIA is preferentially localized within the cortical actin wall. Immuno-electron micrographs of L6 myoblasts cultured for 24 h in DM (DM1). Black dots (immuno-gold particles) within the micrographs indicate the localization of either NM-MHC-IIA or NM-MHC-IIB. (A, B) Representative micrographs showing that NM-MHC-IIA is highly associated with the asymmetrical, actin wall. (B) A higher magnification image reveals that NM-MHC-IIA is localized within the actin wall and is closely associated with the thick subplasmalemmal actin wall. (C) NM-MHC-IIB is more broadly distributed within the cytoplasm of the myoblasts and significantly fewer gold particles are observed within the actin wall. (D) Schematic illustration indicating how NM-MHC-IIA or NM-MHC-IIB immuno-gold particles were quantified. Immuno-gold particles within 2 µm of the plasma membrane were counted in 25–30 randomly selected myoblast pairs. (E) Summary of the localization of NM-MHC-IIA compared to NM-MHC-IIB. Particles within and excluded from the actin wall were counted separately and the percentage of particles within the wall is shown. Immuno-electron micrographs are representative of 2 independent preparations.

it was apparent that NM-MHC-IIA was preferentially associated with and integrated within the actin wall. This observation was confirmed by quantification of the immuno-gold particles along the actin walls of myoblasts at DM1 which revealed that 78.9±10.2% of the NM-MHC-IIA was found within the actin wall compared with only 21.4±9.7% of NM-MHC-IIB (Fig. 6E) a result consistent with Swailes et al. (2006).

Depletion of NM-MHC-IIA impairs the formation of the actin wall and the appearance of vesicles along aligned membranes

Results in Figs. 5 and 6 suggested that NM-MHC-IIA might have a specific role in the organization and assembly of the actin wall. To determine if NM-MHC-IIA was essential for formation of the actin wall structure at the ultrastructural level, myoblasts were treated with si-IIA, or with si-NT and analyzed by EM. Representative micrographs, shown in Fig. 7 illustrates that in contrast to control si-NT treated myoblasts (Fig. 7B), the actin wall is undetectable in myoblasts treated with si-IIA (Fig. 7A) and these myoblasts have a significantly less well-organized actin cytoskeletal structure adjacent to the plasma membrane. Also notable was the irregular contour of the plasma membrane, which was observed in si-IIA treated cells, suggesting that lack of an actin wall results in a more easily deformable plasma membrane. These results demonstrate that siRNA mediated depletion of NM-MHC-IIA from myoblasts severely compromises the organization and assembly of the cortical actin wall.

If depletion of NM-MHC-IIA alters formation of the actin wall, a relatively large and transient structure, then it would be expected that the levels of F-actin in these si-IIA treated myoblasts might also be altered. To determine if this is true, L6 myoblasts were treated with si-IIA or si-NT and the ratios of F/G actin were determined at the indicated times (Fig. 7C). These results show that both the differentiation induced increase in F/G actin ratio and the basal level of F-actin are attenuated following depletion of NM-MHC-IIA (Figs. 7C, D). However, by DM4, the F/G actin ratios of the NM-MHC-II depleted cells had returned to the levels of the control si-NT treated cells. The finding that depletion of NM-MHC-IIA significantly decreased the polymerization of G-actin to F-actin in myoblasts at DM1 is consistent with an important role for NM-MHC-IIA in assembly of the actin wall. These results together with those of Fig. 1D, suggests that the apparent increase in F/G actin ratio observed during the shift in myoblast cultures from GM to DM1, results from assembly of the actin wall, since blocking the formation of the actin wall by depletion of NM-MHC-IIA, eliminated the observed increase in the ratio of F/G actin (Fig. 7B).

Data presented in Fig. 4 suggest that by DM2, numerous gaps occur in the actin wall, which are populated by membrane bound vesicles, which in some cases appeared to be associated with fusion pore-like structures. This finding together with the determination that depletion of NM-MHC-IIA blocks formation of the actin wall, suggested that the appearance of vesicles at the plasma membrane might also be compromised if the actin wall served to either restrict association of or alternatively channeled these vesicular structures to the plasma membrane. To examine this possibility, the numbers of vesicles localized within 1 µm of the plasma membranes were counted in micrographs prepared from myoblasts treated either with the control, non-targeting si-NT or si-IIA. Results from this analysis showed a significant decrease in the number of vesicles localizing within 1 µm of the plasma membrane (Fig. 7E). Measurements of the diameters of the vesicles show that they ranged from 40 to 110 nm and that there was no significant difference in the vesicle diameters between si-NT and si-IIA treated myoblasts. Together these results suggest that NM-MHC-IIA has a role in formation, organization, and maintenance of a novel

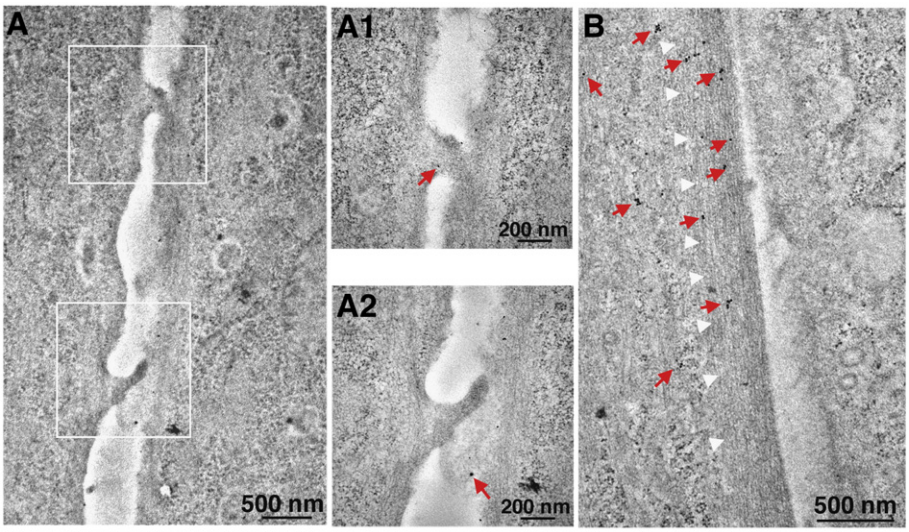

E

Number of vesicles		
Treatment	DM1 (n=100)	DM2 (n=100)
siRNA: NT	26-43	122-217
siRNA: IIA	5-8	11-25

Fig. 7. Depletion of NM-MHC-IIA impairs the formation of the actin wall and the appearance of vesicles along aligned membranes. Immuno-electron micrographs of myoblasts deficient in NM-MHC-IIA (A) or treated with a non-targeting, control siRNA (B). Depletion of NM-MHC-IIA, severely compromises the formation of the actin wall (A), which is barely detectable, loosely organized, and populated by fewer NM-MHC-IIA immuno-gold particles. Areas bounded by the box in panel (A) have been enlarged (A1, A2) to highlight rare immuno-gold particles resulting from incomplete depletion of NM-MHC-IIA. In contrast, myoblasts treated with a non-targeting siRNA have a highly organized and well-developed actin wall (B, white arrows) that is abundantly decorated with NM-MHC-IIA immuno-gold particles (red-arrows). (C) Western blotting to detect F- or G-actin in cell fractions from myoblasts treated with si-NT, si-IIA or si-IIB. (D) Quantification of western blotting data shown in (C) examining F- and G-actin levels in myoblasts treated with siRNAs. (E) Vesicles appearing within 1 mm of the aligned membranes along the entire length of 25–30 randomly selected, aligned myoblasts cultured in DM for 48 h (DM2), were quantified in myoblasts treated either with si-NT (control) or si-IIA. Western blots shown are representative of 4 independent siRNA experiments. Immuno-electron micrographs are representative of 2 independent preparations.

subplasmalemmal actin wall and the temporal appearance of vesicles at the myoblast plasma membrane.

Discussion

Many studies using *Drosophila* as a model system to study muscle development have identified important roles for cytoskeletal proteins in the control and progression of myoblast fusion (Chen and Olson, 2004; Chen and Olson, 2005; Horsley and Pavlath, 2004). In addition, previous studies using immortalized mammalian skeletal muscle myoblasts have identified several actin structures and examined the polarity of actin filaments in differentiating myoblasts (Swailes et al., 2006; Swailes et al., 2004). These studies have also suggested that the NM-MHC-IIA is important for orchestrating the characteristic morphological changes that precede myoblast fusion. The current studies extend these findings and define three unique pre-fusion events in a well-characterized vertebrate myoblast cell line that rely upon the actomyosin cytoskeleton and have fundamentally important roles in regulating myoblast fusion.

First, a distinctive cortical actin wall structure is assembled early during alignment of adjacent myoblasts (Figs. 1 and 2). This actin wall is composed of numerous parallel F-actin filaments that are tightly bundled together to form a structure that has an average thickness of 378 nm. The actin wall borders the plasma membrane and stretches along the entire length of the bipolar aligned myoblasts. Within 24 h of culture in DM, approximately 90% of the cultured myoblasts develop an actin wall structure. In this *in vitro* culture system, the actin wall structure was generally found to be non-randomly distributed within the myoblasts appearing only on one side of the bipolar cell and localized to mid-z planes in confocal images. EM studies revealed further details of the structure of the actin wall and confirmed that it does not arise from cell overlap during fusion. Although at least two previous studies have noted the presence of a highly organized, thick (100–500 nm) subplasmalemmal actin sheet in myoblasts a functional role for this wall in fusion or differentiation was not determined (Lipton, 1977). Biochemically, the timing of the formation of the actin wall is paralleled by a significant increase in the ratio of F-actin to G-actin (Figs. 1D and 7D). This burst of actin polymerization does not appear to result from overt alterations to the normal component of stress fibers present in the myoblasts near the adherent ventral surface of the cells (Figs. 1A, B). As myoblast fusion progresses from DM1 to DM4, the actin wall gradually diminishes and this is paralleled by a decline in the F/G actin ratio to a ratio similar to that found in growth media (Figs. 1D and 7D). Although further

studies will be required to identify the molecular function of the actin wall, its temporal appearance early during differentiation and its cortical location suggests several possibilities for its function. For example, this transient cortical actin wall may serve as a "supportive platform" for the fusion of plasma membranes by providing some rigidity for alignment between adjacent, elongating myoblasts. Consistent with this is the observation that depletion of NM-MHC-IIA not only alters the formation of an actin wall, but also results in a more irregular plasma membrane (Fig. 7A). Alternatively or in addition, this cortical actin wall may serve as a temporal barrier to impede the movement of vesicles containing membrane fusion proteins to the plasma membrane until the myoblasts are completely aligned and competent to fuse. Consistent with this proposal, structures called actin "foci" which appear at sites of fusion in *Drosophila* myoblasts have recently been shown to disintegrate just prior to membrane fusion (Kesper et al., 2007; Kim et al., 2007; Richardson et al., 2007). These findings suggest that actin foci may temporally impede fusion during the late phase of the fusion process in addition to providing directionality for microtubule-mediated vesicle trafficking during the early phase of the fusion process (Kim et al., 2007; Richardson et al., 2007). The studies described in this report suggest that in cultured vertebrate myoblasts, a similar actin-enriched structure may form to temporally regulate fusion. While it is tempting to speculate that actin "foci" and the actin wall may share some functional similarity, additional biochemical and functional characterization of these structures will be required to support this proposal.

The second major finding of these studies is that the motor activities of NM-MHC-IIA are critical for the formation of the actin wall. This finding is supported by results showing that NM-MHC-IIA is highly enriched within the actin wall (Fig. 6) and that depletion of NM-MHC-IIA inhibits formation of the cortical actin wall (Fig. 7) and myoblast fusion (Fig. 5). In addition, inhibition of myosin motor activity by blebbistatin (see Fig. S3 in the Supplementary material) or expression of a dominant negative RLC (see Fig. S4 in the Supplementary material) inhibits formation of the actin wall. Together these data suggest that the motor activity of NM-MHC-IIA is specifically required for formation of the actin wall. This finding is consistent with the recently identified role of NM-MHC-IIA in organization and bundling of actin filaments in the lamellipodia of migrating cells (Choi et al., 2008). Also, as NM-MHCs have been shown to form small bipolar mini-filaments within dense cortical actin structures that mediate network contraction (Clarke and Spudich, 1974; Hynes et al., 1987; Laevsky and Knecht, 2003; Pellegrin and Mellor, 2007; Sheetz et al., 1986) it is possible that NM-MHC-IIA is not only involved in formation of the actin wall through its ability to translocate actin filaments to form the wall, but also regulates its contractility by binding to filaments and exerting tension (Conti and Adelstein, 2008). Surprisingly, we also found that depletion of NM-MHC-IIA resulted in myoblasts that are unable to fuse to form multinucleated myotubes (Fig. 5), yet are able to adhere to culture dishes, elongate to form bipolar cells, and align normally when cultured in DM. The inability of NM-MHC-IIA deficient cells to fuse is consistent with a previous study (Swailes et al., 2006). However, this study also suggested that depletion of NM-MHC-IIA inhibits myoblast fusion by preventing cell to cell attachment and bipolar shape formation, while our results suggest that normal bipolar shape formation is unaffected and rather define a critical role for NM-MHC-IIA in formation of an actin wall structure that is a necessary prerequisite for myoblast fusion. The reason for this discrepancy is unclear, but could be due to differences in cell lines or culture conditions. Collectively the results of our studies demonstrate that NM-MHC-IIA has a central role in the formation and/or maintenance of a non-uniformly distributed, cortical actin wall, which is an essential early prerequisite for myoblast fusion.

Finally, our results show that prior to the rapid myoblast fusion phase, which occurs between DM2 and DM4, the cortical actin wall reorganizes and gaps become apparent within the wall (Fig. 3, see Movie 2 in the Supplementary material). The temporal appearance of these gaps in DM2 myoblasts corresponds with the arrival of numerous membrane bound vesicles at the plasma membrane region, where the vesicles appear to cluster within the gaps forming in the actin wall (Figs. 3 and 4). Even though subplasmalemmal vesicles have been reported in primary myoblasts derived from quail (Lipton and Konigsberg, 1972) and chick embryos (Kalderon and Gilula, 1979) as well as in the L6 myoblast cell line (Engel et al., 1986), their temporal association with gaps occurring in a cortical actin wall structure has not been previously described. Intriguingly, as these vesicles reach the plasma membrane they appear to align with vesicles in the juxtaposed myoblast to form symmetrical pairs similar to those previously observed in differentiating *Drosophila* myoblasts (Doberstein et al., 1997; Kim et al., 2007). In addition, Kim et al identified electron dense vesicles coated with actin and suggested that the presence of actin on these vesicles indicated a role for the actin cytoskeleton in trafficking these vesicles to sites of fusion. In *Drosophila*, vesicle pairing was suggested to be an essential prefusion structure that serves to traffic and cluster membrane proteins to the plasma membrane for cell–cell fusion. Our current studies show that the average diameter of the vesicles appearing in the L6 myoblasts ranged between 40 and 110 nm, a result that is comparable to vesicles identified in chick embryo myoblasts having a diameter of 0.1–0.2 μm (100–200 nm) (Kalderon and Gilula, 1979). The appearance of these vesicles within gaps in an actin wall structure extends this finding suggesting that the actin wall may serve to temporally restrict the association of the vesicles with the plasma membrane until the myoblasts have elongated and aligned before forming cell–cell contacts for fusion (Fig. 8). This spatial and temporal restriction may result in clustering of vesicles containing membrane fusion proteins at the plasma membrane in actin wall gaps to ensure efficient communication to initiate formation of fusion pores. This suggestion is supported by a recent study showing that NM-MHC-IIA has a direct role in fusion pore expansion to allow exocytosis of neurotransmitters (Neco et al., 2008). Depletion of NM-MHC-IIA not only abrogated formation of the actin wall but it also blocked the appearance of vesicles at the plasma membrane (Fig. 7). This apparently paradoxical observation suggests that NM-MHC-IIA is not only important for formation of an actin wall but is also required to move vesicles to the plasma membrane once the actin wall is disrupted (Fig. 8). Several previous studies support a direct role for NM-MHC-IIA in vesicle movement and trafficking of plasma membrane proteins such as Glut-4, CXCR4, and E-cadherin to the plasma membrane (Andzelm et al., 2007; Conti and Adelstein, 2008; Conti et al., 2004; Fulcher et al., 2008; Ivanov et al., 2007; Rey et al., 2007; Shewan et al., 2005; Steimle et al., 2005).

In summary our studies have identified a novel, non-uniform, cortical actin wall structure and demonstrate that development of an actin wall is critically dependent on the motor activities of NM-MHC-IIA. In addition, these results suggest that formation of an actin wall structure temporally restricts the initiation of membrane fusion until myoblasts have aligned and elongated to become bipolar cells.

Materials and methods

Cell culture and chemicals

Rat L6 or C2C12 myoblasts were cultured in growth medium (GM) composed of minimal essential medium (Invitrogen) supplemented with 10% FBS 2 mM glutamine, 100 U/ml penicillin, and 100 μg/ml streptomycin, in a H_2O-saturated 5% CO2 atmosphere at 37 °C (growth medium, GM). For all experiments in this report the myoblasts were cultured and maintained in growth medium (GM) and where indicated differentiated by removal of GM, followed by 2 washes using differentiation medium (DM) which is identical to GM except, FBS is reduced to 2%, and then culture of the myoblasts in fresh DM for

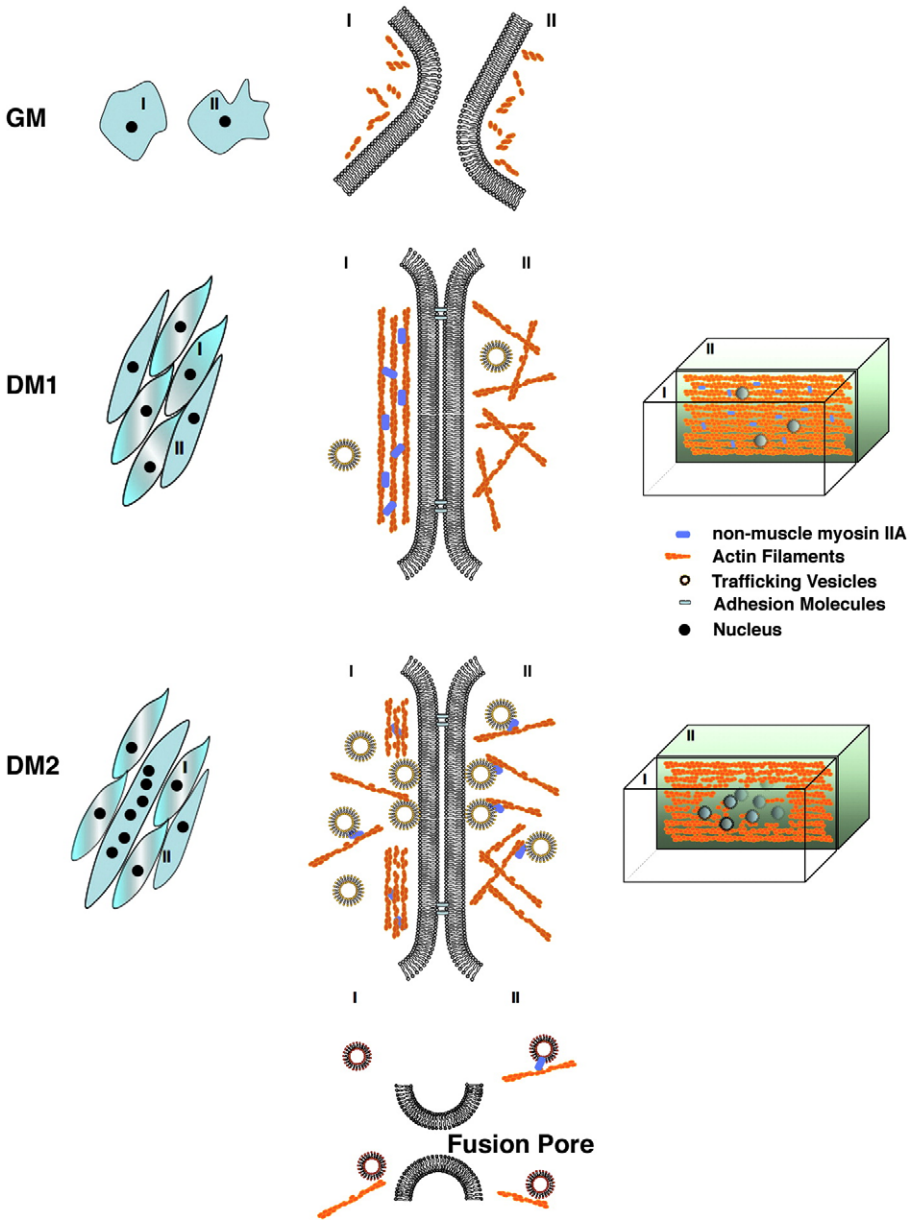

Fig. 8. Temporal and spatial events during skeletal muscle myoblast fusion. When cultured in growth medium (GM) myoblasts are irregularly shaped, with a central nucleus and loosely organized cytoplasmic actin filaments. Upon culture in differentiation medium for 24 h (DM1), the myoblasts elongate, assume a bipolar orientation and a highly organized actin wall forms in aligned myoblasts. Subsequent to assembly of the actin wall, a second phase of actin reorganization occurs between 24 and 48 h of culture in DM (DM2, DM4) to result in the appearance of gaps within the actin wall. The formation of gaps within the actin wall is accompanied by the trafficking of membrane bound vesicles to these gap regions where they pair with vesicles in the cortical region of the juxtaposed myoblast. Subsequent to vesicle pairing, cell–cell contacts and localized fusion pores appear which then expand laterally as fusion progresses to result in a multinucleated, syncytial cell.

24 h (DM1), 48 h (DM2) or 96 h (DM4). Blebbistatin was from Calbiochem (La Jolla, CA). Mouse anti-HA antibody was from Covance (Berkeley, CA). Mouse anti-skeletal myosin heavy chain (fast, MY-32) antibody, mouse anti-vinculin antibody and protease inhibitors cocktail were from Sigma (St Louis, MI). Alexa Fluor 488 phalloidin, Texas Red-X phalloidin and Hoechst 33342 were from Molecular Probes (Eugene, OR). Mouse anti-nonmuscle actin (cytoskeleton, Inc) and cytochalasin D (Sigma, MI) were a gift from Dr. Susan Gunst (Indiana University School of Medicine). All electron microscopy reagents were provided by Indiana University EM center. Polyclonal antibodies to nonmuscle myosin heavy chains IIA and IIB were generated and characterized in this laboratory (Blue et al., 2002; Krits et al., 2002). NM-MHC-IIC antibody was a kind gift from Dr. Robert Wysolmerski. The GFP-NM-MHC-IIA plasmid was kind a gift from Dr. Robert Adelstein.

Immunofluorescence

Cells for immunofluorescence microscopy were plated on 24×24 mm glass coverslips (Fisher Scientific) and cultured for the indicated times. Cells were fixed with 4% paraformaldehyde in PBS, permeabilized with 0.2% Triton X-100 and stained using the indicated primary and secondary antibodies coupled to Alexa Fluor 488 or Texas Red-X phalloidin (Invitrogen). Nuclei were stained by Hoechst 33342 (Invitrogen).

Analysis of F-actin and G-actin

The assay was carried out essentially as described previously (Zhang et al., 2005). Briefly, cells were homogenized in F-actin stabilization buffer and the supernatants are collected following ultra-

centrifugation (100,000 *g*, 1 h, 37 °C). The pellets were resuspended in ice-cold distilled water plus 1 μM cytochalasin-D and then incubated on ice for 1 h to dissociate F-actin. Supernatant (G-actin) and pellet (F-actin) fractions were diluted 50 times and analyzed by immunoblotting using polyclonal anti-nonmuscle actin antibody (Cytoskeleton, Inc). The ratio of F-actin to G-actin was determined by scanning densitometry of the western blots.

Microscopy and image processing

Phase contrast images were acquired using an inverted microscopy (10×/0.25 NA, A10PL objective, CK2, Olympus) with a CCD camera (PL A662, Pixelink) using Pixelink Capture software (Pixelink). Confocal images were collected right after sample preparation on a Zeiss laser confocal microscope LSM 510 with Apo ×63 objective lens (NA 1.4, oil) and then analyzed using Zeiss LSM Image software in Expert mode (Carl Zeiss, Inc.). Alexa-488 labeled proteins were excited with a 488 nm argon laser and fluorescence emissions were collected at 500–530 nm. The optical pinhole was set to resolve optical sections of ~1 mm in cell thickness. All images were imported and organized in Photoshop (Adobe) and brightness and contrast were adjusted to the same extent for each image panel. Three-dimensional (3D) reconstructions were produced using Zeiss LSM Image Browser V4.0 (Carl Zeiss, Inc) and MetaMorph (Molecular Devices) software.

Conventional and immuno-EM

For conventional EM, cells were grown on Thermonox coverslips (Nalge Nunc International) and fixed in 2% glutaraldehyde together with 2% paraformaldehyde in 0.1 M phosphate buffer for 4 h. The cells were rinsed in phosphate buffer and then post-fixed for 1 h in 2% osmium tetroxide in 0.1 M phosphate buffer. After rinsing in 0.1 M phosphate buffer, the cells were dehydrated and embedded before en face sectioning. Sections 70 nm in thickness were stained with uranyl acetate and lead citrate. For Immuno-EM, myoblasts were grown on Thermonox cover slips and fixed overnight in 4% paraformaldehyde prepared in 0.1 M phosphate, pH 7.4. After incubation in 50 mm ammonium chloride cacodylate/sucrose buffer (0.1 M cacodylate with 3.5% sucrose pH 7.4), the cells were then stained in 2% uranyl acetate and dehydrated. The cells were infiltrated with LR Gold and 70 nm thick *en face* sections were incubated with affinity purified primary antibodies, washed and then incubated with secondary goat anti-rabbit antibodies conjugated to 10 nm colloidal goal particles at 1:40 (Aurion). The sections were washed, post-fixed in 2% glutaraldehyde, stained with saturated uranyl acetate and viewed with a Tecnai G2 12 Bio Twin Transmission Electron Microscope (FEI, Hillsboro, OR) at 80KV. Digital analysis was performed using Image J (NIH). To determine the percentage of immuno-gold particles within the actin wall, immuno-gold particles within 4 adjacent, 2 mM×2 mM squares were counted (area=4×106 nm^2) in 25–30 randomly selected cell pairs of aligned myoblasts from 3 independent preparations. Each square was placed such that one side was aligned to the plasma membrane. Particles within and excluded from the actin wall were counted separately and the percentage of particles within the wall was calculated by dividing the number of particles in the wall by the total number of particles. For both TEM and immuno-EM, each sample was coded to allow for blinded examination and at least 30 micrographs per sample were examined. Examination of these micrographs confirmed that the ultra-structure of the cortical actin wall previously identified by convention EM was indistinguishable from myoblasts prepared from immuno-EM. This comparison suggested that preparation of myoblast cultures for immuno-EM does not significantly alter the appearance or location of the actin wall structure although the plasma membrane in the immuno-EMs is not easily discernable due to permeabilization of the cells.

Myoblast fusion index and nuclear distribution analysis

The fusion index was determined by quantifying the number of multinucleated cells having more than four nuclei that express skeletal myosin heavy chain (Sk MHC) after culture in GM, DM2 or DM4. The distribution of nuclei in sk-MHC positive cells was determined by directly counting of the number of nuclei in fused myoblasts with more than 4 nuclei and expressing sk-MHC. At least 20 random view fields were selected and the experiments were repeated 3 times.

Western blotting and quantification

Cellular proteins were extracted either with NP-40 lysis buffer (1% NP-40, 300 mM NaCl, 0.5 mM EGTA, 50 mM MgCl2, 10% glycerol and 20 mM MOPS, pH 7) or 2% SDS lysis buffer (2% SDS, 100 mM NaCl, 50 mM Tris–HCl, PH 7.4) supplemented with a protease cocktail and analyzed by western blotting. Protein quantification was performed using Fujifilm LSM-1000plus software. The chemiluminescent emission from both the target of interest and internal loading control has been automatically and manually tested in the linear range. The average emission of four randomly selected empty areas was used as a film background control. For each experiment, at least four independent preparations have been examined.

siRNA

Transfection reagent (DharmaFect-1), non-targeting siRNAs and siRNAs for depletion of NM-MHC-IIA or IIB were from Dharmacon (Lafayette, CO). The sequences are: si-IIA 5′-UGACAGAGAUGGAGACUAU, 5′GGGAUGAGCUGGCCGAUGA, 5′GAAGGUGGCUGC-CUAUGAU; si-IIB 5′GGGCAUCUCUGCUCGCUAU, 5′GGACUCAUCUAUACUUACU, 5′GAUGAUCUCGGAUUUAGAA, 5′GAAACUGGACGGUGAAACA. These siRNA oligos were tested individually using western blotting and qRT-PCR to confirm that they efficiently and specifically deplete expression of either IIA or IIB in L6 cells (rat siRNAs) in either growth or differentiation medium (both lacking penicillin and streptomycin) (see Fig. S5 in the Supplementary material). In addition, to exclude the "off-target" effects of the siRNAs, each selected siRNAs were tested in a functional assay (myoblast fusion) individually. For all siRNAs, the transfection efficiency and transfection conditions were optimized using fluorescently tagged siRNAs. The optimized protocol resulted in a reproducible transfection efficiency of greater than 95% in L6 myoblasts.

Transfection

Rat L6 skeletal muscle myoblasts were plated to achieve a low sub-confluent density in antibiotic-free complete medium (DMEM +10% FBS). The cells were incubated at 37 °C with 5% CO2 until cell density had doubled but was sub-confluent. For transfections in 6-well culture dishes, a 2 μM siRNA solution in 1× siRNA Buffer was prepared and then 10 μl is added with gentle mixing to a separate tube containing 4 μl of DharmaFECT™1 in 200 μl serum-free medium. After 20 min at room temperature, 1.6 ml antibiotic-free complete medium was added and 100 μl was added to each well. The cells were incubated for 24 h in the transfection mixture and then changed into antibiotic-free differentiation medium (DM) containing the same siRNAs. The relative level of mRNA knockdown (see Fig. S5 in the Supplementary material) was determined at 0, 24, 48 and 144 h after transfection. Control experiments were conducted in parallel using scrambled, non-targeting siRNAs, or transfection reagent only (DharmaFECT™1). Western blotting and real-time quantitative RT-PCR were performed to determine the relative levels of knockdown of each NM-MHC isoform (see Fig. S5 in the Supplementary material).

Statistical analysis

All experiments were carried out using independent cell transfections, in triplicate. Statistical analysis was performed using Student's *t*-test.

Acknowledgments

This work was supported by grants from the National Institutes of Health (NHLBI HL54118 and DK062810) to P. J. G. We thank Dr. Vincent H. Gattone and Janice Pennington for EM technical support and Dr. Susan Gunst for assistance with the F/G actin assay and MetaMorph™ software. We also thank Dr. Fred Pavalko for immuno-fluorescence microscopy support, Dr. Jiliang Zhou and Min Zhang for qRT-PCR support and members of the Gallagher, Herring and Elmendorf lab as well as Dr. Elizabeth Chen (JHU) for useful discussions.

Appendix A. Supplementary data

Supplementary data associated with this article can be found, in the online version, at doi:10.1016/j.ydbio.2008.10.035.

References

Andzelm, M.M., Chen, X., Krzewski, K., Orange, J.S., Strominger, J.L., 2007. Myosin IIA is required for cytolytic granule exocytosis in human NK cells. J. Exp. Med. 204, 2285–2291.

Berger, S., Schafer, G., Kesper, D.A., Holz, A., Eriksson, T., Palmer, R.H., Beck, L., Klambt, C., Renkawitz-Pohl, R., Onel, S.F., 2008. WASP and SCAR have distinct roles in activating the Arp2/3 complex during myoblast fusion. J. Cell. Sci. 121, 1303–1313.

Blue, E.K., Goeckeler, Z.M., Jin, Y., Hou, L., Dixon, S.A., Herring, B.P., Wysolmerski, R.B., Gallagher, P.J., 2002. 220- and 130-kDa MLCKs have distinct tissue distributions and intracellular localization patterns. Am. J. Physiol., Cell Physiol. 282, C451–460.

Chen, E.H., Olson, E.N., 2004. Towards a molecular pathway for myoblast fusion in *Drosophila*. Trends Cell Biol. 14, 452–460.

Chen, E.H., Olson, E.N., 2005. Unveiling the mechanisms of cell–cell fusion. Science. 308, 369–373.

Chen, E.H., Grote, E., Mohler, W., Vignery, A., 2007. Cell–cell fusion. FEBS Lett. 581, 2181–2193.

Choi, C.K., Vicente-Manzanares, M., Zareno, J., Whitmore, L.A., Mogilner, A., Horwitz, A. R., 2008. Actin and alpha-actinin orchestrate the assembly and maturation of nascent adhesions in a myosin II motor-independent manner. Nat. Cell Biol. 10, 1039–1050.

Clarke, M., Spudich, J.A., 1974. Biochemical and structural studies of actomyosin-like proteins from non-muscle cells. Isolation and characterization of myosin from amoebae of Dictyostelium discoideum. J. Mol. Biol. 86, 209–222.

Conti, M.A., Adelstein, R.S., 2008. Nonmuscle myosin II moves in new directions. J. Cell. Sci. 121, 11–18.

Conti, M.A., Even-Ram, S., Liu, C., Yamada, K.M., Adelstein, R.S., 2004. Defects in cell adhesion and the visceral endoderm following ablation of nonmuscle myosin heavy chain II-A in mice. J. Biol. Chem. 279, 41263–41266.

Doberstein, S.K., Fetter, R.D., Mehta, A.Y., Goodman, C.S., 1997. Genetic analysis of myoblast fusion: blown fuse is required for progression beyond the prefusion complex. J. Cell Biol. 136, 1249–1261.

Engel, L.C., Egar, M.W., Przybylski, R.J., 1986. Morphological characterization of actively fusing L6 myoblasts. Eur. J. Cell Biol. 39, 360–365.

Erickson, M.R., Galletta, B.J., Abmayr, S.M., 1997. *Drosophila* myoblast city encodes a conserved protein that is essential for myoblast fusion, dorsal closure, and cytoskeletal organization. J. Cell Biol. 138, 589–603.

Fowler, W.E., Aebi, U., 1983. A consistent picture of the actin filament related to the orientation of the actin molecule. J. Cell Biol. 97, 264–269.

Fulcher, F.K., Smith, B.T., Russ, M., Patel, Y.M., 2008. Dual role for myosin II in GLUT4-mediated glucose uptake in 3T3-L1 adipocytes. Exp. Cell Res. 314, 3264–3274.

Gallagher, P.J., Jin, Y., Killough, G., Blue, E.K., Lindner, V., 2000. Alterations in expression of myosin and myosin light chain kinases in response to vascular injury. Am. J. Physiol., Cell Physiol. 279, C1078–1087.

Horsley, V., Pavlath, G.K., 2004. Forming a multinucleated cell: molecules that regulate myoblast fusion. Cells Tissues Organs 176, 67–78.

Hynes, T.R., Block, S.M., White, B.T., Spudich, J.A., 1987. Movement of myosin fragments in vitro: domains involved in force production. Cell 48, 953–963.

Ivanov, A.I., Bachar, M., Babbin, B.A., Adelstein, R.S., Nusrat, A., Parkos, C.A., 2007. A unique role for nonmuscle myosin heavy chain IIA in regulation of epithelial apical junctions. PLoS ONE 2, e658.

Kalderon, N., Gilula, N.B., 1979. Membrane events involved in myoblast fusion. J. Cell Biol. 81, 411–425.

Kesper, D.A., Stute, C., Buttgereit, D., Kreiskother, N., Vishnu, S., Fischbach, K.F., Renkawitz-Pohl, R., 2007. Myoblast fusion in *Drosophila melanogaster* is mediated through a fusion-restricted myogenic-adhesive structure (FuRMAS). Dev. Dyn. 236, 404–415.

Kim, S., Shilagardi, K., Zhang, S., Hong, S.N., Sens, K.L., Bo, J., Gonzalez, G.A., Chen, E.H., 2007. A critical function for the actin cytoskeleton in targeted exocytosis of prefusion vesicles during myoblast fusion. Dev. Cell. 12, 571–586.

Krits, I., Wysolmerski, R.B., Holliday, L.S., Lee, B.S., 2002. Differential localization of myosin II isoforms in resting and activated osteoclasts. Calcif. Tissue Int. 71, 530–538.

Laevsky, G., Knecht, D.A., 2003. Cross-linking of actin filaments by myosin II is a major contributor to cortical integrity and cell motility in restrictive environments. J. Cell. Sci. 116, 3761–3770.

Lipton, B.H., 1977. A fine-structural analysis of normal and modulated cells in myogenic cultures. Dev. Biol. 60, 26–47.

Lipton, B.H., Konigsberg, I.R., 1972. A fine-structural analysis of the fusion of myogenic cells. J. Cell Biol. 53, 348–364.

Luo, L., Liao, Y.J., Jan, L.Y., Jan, Y.N., 1994. Distinct morphogenetic functions of similar small GTPases: *Drosophila* Drac1 is involved in axonal outgrowth and myoblast fusion. Genes Dev. 8, 1787–1802.

Massarwa, R., Carmon, S., Shilo, B.Z., Schejter, E.D., 2007. WIP/WASp-based actin-polymerization machinery is essential for myoblast fusion in *Drosophila*. Dev. Cell. 12, 557–569.

Neco, P., Fernandez-Peruchena, C., Navas, S., Gutierrez, L.M., de Toledo, G.A., Ales, E., 2008. Myosin II contributes to fusion pore expansion during exocytosis. J. Biol. Chem. 283, 10949–10957.

Pellegrin, S., Mellor, H., 2007. Actin stress fibres. J. Cell. Sci. 120, 3491–3499.

Rey, M., Valenzuela-Fernandez, A., Urzainqui, A., Yanez-Mo, M., Perez-Martinez, M., Penela, P., Mayor Jr., F., Sanchez-Madrid, F., 2007. Myosin IIA is involved in the endocytosis of CXCR4 induced by SDF-1alpha. J. Cell. Sci. 120, 1126–1133.

Richardson, B.E., Beckett, K., Nowak, S.J., Baylies, M.K., 2007. SCAR/WAVE and Arp2/3 are crucial for cytoskeletal remodeling at the site of myoblast fusion. Development. 134, 4357–4367.

Schafer, G., Weber, S., Holz, A., Bogdan, S., Schumacher, S., Muller, A., Renkawitz-Pohl, R., Onel, S.F., 2007. The Wiskott–Aldrich syndrome protein (WASP) is essential for myoblast fusion in *Drosophila*. Dev. Biol. 304, 664–674.

Sheetz, M.P., Block, S.M., Spudich, J.A., 1986. Myosin movement in vitro: a quantitative assay using oriented actin cables from Nitella. Methods Enzymol. 134, 531–544.

Shewan, A.M., Maddugoda, M., Kraemer, A., Stehbens, S.J., Verma, S., Kovacs, E.M., Yap, A.S., 2005. Myosin 2 is a key Rho kinase target necessary for the local concentration of E-cadherin at cell–cell contacts. Mol. Biol. Cell 16, 4531–4542.

Steimle, P.A., Fulcher, F.K., Patel, Y.M., 2005. A novel role for myosin II in insulin-stimulated glucose uptake in 3T3-L1 adipocytes. Biochem. Biophys. Res. Commun. 331, 1560–1565.

Swailes, N.T., Knight, P.J., Peckham, M., 2004. Actin filament organization in aligned prefusion myoblasts. J. Anat. 205, 381–391.

Swailes, N.T., Colegrave, M., Knight, P.J., Peckham, M., 2006. Non-muscle myosins 2A and 2B drive changes in cell morphology that occur as myoblasts align and fuse. J. Cell. Sci. 119, 3561–3570.

Zhang, W., Wu, Y., Du, L., Tang, D.D., Gunst, S.J., 2005. Activation of the Arp2/3 complex by N-WASp is required for actin polymerization and contraction in smooth muscle. Am. J. Physiol., Cell Physiol. 288, C1145–1160.